Exploring the cellular uptake of hectorite clay mineral and its drug carrier capabilities

Monica Notarbartolo,[*,a] Marina Massaro,[a] Raquel de Melo Barbosa,[b] Carlotta Emili,[c] Leonarda Francesca Liotta,[d] Paola Poma,[a] Françisco M. Raymo,[e] Rita Sànchez-Espejo,[b,f] Riccardo Vago,[c,g] César Viseras-Iborra,[b,f] Serena Riela[*,a]

[a]Dipartimento di Scienze e Tecnologie Biologiche Chimiche e Farmaceutiche (STEBICEF), Università degli Studi di Palermo, Parco d'Orleans II, Ed. 17, 90128 Palermo, Italy. Email: monica.notarbartolo@unipa.it; serena.riela@unipa.it

[b]University of Granada, Department of Pharmacy and Pharmaceutical Technology, Faculty of Pharmacy, 18071, Granada, Spain.

[c]Urological Research Institute, Division of Experimental Oncology, IRCCS San Raffaele Scientific Institute, Milano, Italy.

[d]Istituto per lo Studio dei Materiali Nanostrutturati (ISMN)-CNR, Via Ugo La Malfa 153, Palermo 90146, Italy.

[e]Laboratory for Molecular Photonics, Department of Chemistry, University of Miami, 1301 Memorial Drive, Coral Gables 33146-0431, Florida, USA.

[f]Andalusian Institute of Earth Sciences, CSIC-UGR, 18100 Armilla, Granada, Spain.

[g]Università Vita-Salute San Raffaele, Milano, Italy.

5462 words

1 Table

7 Figures

Abstract

In the last years, the use of clay minerals for pharmaceutical purposes has increased due to their interesting properties. Hectorite (Ht) is a clay belonging to the smectite group which has attracted attention for applications in biology, tissue engineering and as drug carrier and delivery system. However, the mechanisms involved in Ht cellular uptake and transport into cells, are still unclear. Herein, we used a labelled Ht (Ht/**1Cl**) to study both the cellular uptake, by confocal laser scanning microscopy, and internalization pathways involved in the cellular uptake, by various endocytosis-inhibiting studies and fluorescence microscopy. These studies highlighted that Ht can penetrate the cellular membrane, localizing mainly in the cytoplasm. The main intracellular transport mechanisms are the ATP-dependent ones and those where filaments and microtubules are involved. Finally, as proof of concept for the potential of Ht as carrier system, we envisaged the covalent grafting of the anticancer molecule methotrexate (MTX), chosen as model, to obtain the Ht-MTX nanomaterial. The covalent linkage was confirmed by several techniques and the morphology of the obtained nanomaterial was imaged by SEM and TEM investigations. The kinetic release of the drug

from the Ht-MTX nanomaterial in physiological conditions was studied as well. Furthermore, cytotoxic studies on different cell lines, namely, HL-60, HL-60R, MCF-7, 5637, UMUC3 and RT112 showed that Ht could be a promising material for anticancer therapy.

KEYWORDS: hectorite, cellular uptake, cellular internalization, methotrexate, cytotoxicity.

1. Introduction

The use of clay minerals for pharmacological purposes in renowned since ancient times. Since prehistory, clay minerals were widely used for the treatment of different pathologies such as infections, pains, aches, and food poisoning. The *terra Lemnia* is the earliest example of a clay mineral, Kaolin, recognized for its therapeutic properties, used by ancient Greek people.[1-3]

Eventually, due to the extensive use of clay minerals as pharmaceuticals, during Renaissance they were classified as drug. Up to now, clay minerals are used for medical and pharmaceutical purposes as additives or active species according to the different concentration used.[4-6]

From a chemical point of view, clay minerals are phyllosilicate characterized by layered structures constituted by SiO_4 tetrahedral sheets linked to neighboring tetrahedra by sharing three corners. The combination of these sheets results in a hexagonal network; the remaining fourth oxygen of each tetrahedron belongs also to adjacent octahedral sheet, usually consisting of magnesium, iron or aluminum in six-fold coordination with oxygen from the tetrahedral sheet and with hydroxyl groups. Depending on the different arrangement of the tetrahedral and octahedral sheets clay minerals can be classified as 1:1 and 2:1 phyllosilicate. The 1:1 phyllosilicates have one tetrahedral and one octahedral sheet per clay layer;[7] whereas in the 2:1 clay minerals, each layer consists of one octahedral sheet sandwiched between the two tetrahedral sheets.

Hectorite (Ht) is a natural layered magnesium-lithium silicate belonging to the smectite group (2:1). It is a trioctahedral clay mineral with an ideal chemical formula of $Na_{0.3}Mg_{2.7}Li_{0.3}Si_4O_{10}(OH)_2$. Chemically it is constituted by different layers of Si–O–Mg(Li) –O–Si– with hydrated cations (e.g. Na^+, Li^+) in the interlayer space (Figure 1).[8]

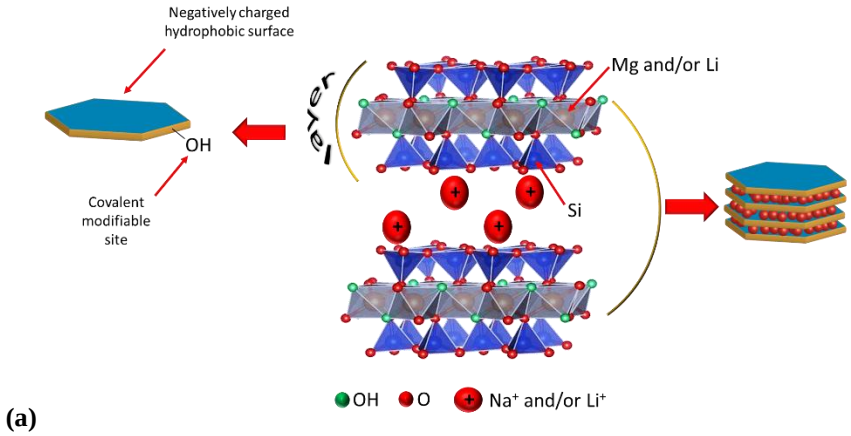

(a)

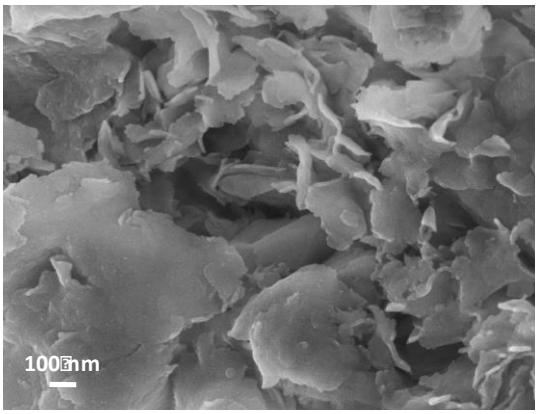

(b)

Figure 1. (a) Representation of Ht structure; (b) SEM image of Ht.

Hectorite nanolayers, as others 2:1 clay minerals, show negative charges on the basal faces (siloxane groups) and pH-dependent charge on the edges. In addition, the siloxane groups confer hydrophobic properties to the basal faces, while the silanol groups present at the edges can be chemically modified.[9, 10] Hectorite, similarly to other clays of smectite group, present a high cation exchange capacity (CEC) that in this case ranged from 50 to 150 mmol/100 g in a pH range from 6 to 13,[11] and specific surface area about 350 m^2/g.[12]

Recent studies have shown the great potentiality of Ht as drug carrier for application in biological field, regenerative medicine, and tissue engineering.[13] Its peculiar physico-chemical properties, such as high swellability and CEC, delamination, and the typical in water arrangement of the "house-of-cards" structure, has enabled the synthesis of several nanomaterials of biological and biomedical interest.

Considering the emerging role fulfilled by clay minerals in drug carrier and delivery fields,[14, 15] the understanding of their internalization mechanisms, uptake, distribution, and localization in living cells, is fundamental to develop smart systems for the treatment of different pathologies.[16]

Up to now, few studies reported the internalization of 1:1 clay minerals,[9, 17] but to the best of our knowledge, the mechanism of cellular uptake of Ht is poorly understood.

Herein we explore the cellular uptake of Ht in terms of distribution and localization into non-tumoral hTERT RPE-1 and MCF-7 breast cancer cells by confocal laser scanning microscopy

(CLSM) experiments. The internalized pathway of Ht in MCF-7 living cells, by various endocytosis-inhibiting studies and fluorescence microscopy was also investigated. To achieve this goal, we labeled Ht with a synthetic fluorescent probe (**1Cl**).[18, 19]

Successively, as proof of concept for the biological applications of Ht, we investigated its interaction with methotrexate (MTX) molecules, chosen as anticancer drug model. Because of no complexation (by electrostatic attraction interactions or intercalation in the interlayer spaces) occurs between MTX and Ht, the MTX molecules were covalently linked to Ht edges (Ht-MTX) by conventional organosilane chemistry, usually adopted for clay modifications. The nanomaterial obtained was characterized by several techniques and its morphology was investigated by scanning electron microscopy (SEM) and high annular angle dark field/scanning transmission electron microscopy (HAADF/STEM) measurements which conformed the covalent linkage of MTX onto Ht edges. The kinetic release of MTX from Ht in different media was investigated as well.

Finally, the cytotoxic effects of the Ht-MTX carrier were also evaluated on different cancer cell lines, namely acute myeloid leukemia (HL60) and its multidrug resistance variant (HL60-R), breast (MCF-7) and bladder (5637, UMUC3 and RT112) cancer cell lines. This work breaks a lance in favor of the use of Ht as drug carrier.

2. Results and Discussion

The cellular uptake of Ht was assessed by CLSM experiments in living cells and its internalized pathway was investigated by various endocytosis-inhibiting studies by fluorescence microscopy. Considering lack of intrinsic fluorescence in Ht, the clay was labelled with a fluorescent coumarin chromophore combined with a switchable halochromic oxazine (**1Cl**) to obtain a fluorescent Ht/**1Cl**,as already reported by us for other clays.[18] The amount of **1Cl** loaded onto Ht/**1Cl** was ca. 2 wt%. **1Cl** is a synthetic fluorescent probe that possesses the peculiarity of shifting its emission band in response to appropriate external stimuli.[18]

2.1. Uptake studies

Firstly, the cellular uptake of the labelled Ht/**1Cl** was studied by confocal microscopy on two different cell lines, namely the living non-tumor hTERT RPE-1 cells and MCF-7 breast cancer ones. Live cells were incubated with labelled Ht/**1Cl** (10 μM of **1Cl** corresponding to [Ht/**1Cl**] = 180 μg mL^{-1}) at different times (1, 3 and 6 hours). As shown in Figure 2a (A and E) the uptake of the clay into both cells can be clearly observed after only one hour of incubation as highlighted by the blue fluorescence signal localized around the cell nucleus. By increasing the incubation time, the clay shows a heterogeneous distribution in the cytoplasm with aggregates in some specific regions of the cell, localizing mainly in the perinuclear region (Figure 2a B, C, F, G). Similar to

other clays, for example halloysite,[20] accumulation in the cell nuclei is not observed even after prolonged incubation time, indicating that pristine Ht cannot penetrate cell nuclei.

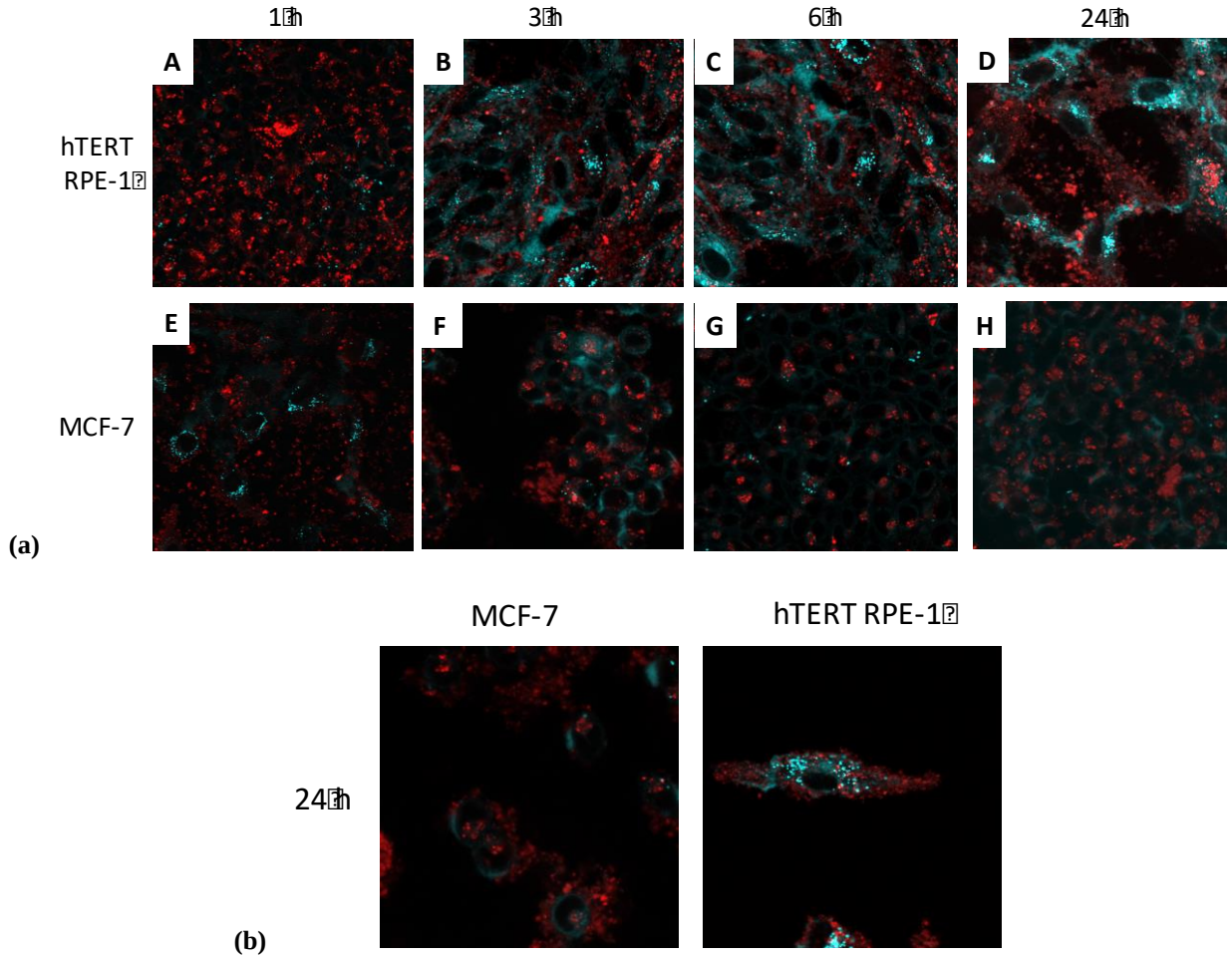

Figure 2. Confocal microscope images of the hTERT RPE-1 and MCF-7 cell lines. Cells were incubated with Ht/1Cl nanomaterial (10 μM of 1Cl corresponding to [Ht/1Cl] = 180 μg mL^{-1}) for 1, 3, 6 and 24 hours. The images were recorded under excitation at 405 and 595 nm. (a) Magnification 40×. (b) Magnification 100×.

However, after 24 h of incubation (Figure 2a D, H, Figure 2b), although both cells showed that the clay is distributed around the nucleus at the same time, the Ht accumulation in a particular portion of the cell occurs. As a consequence, a clear change in the cellular organization is observed with an increase in the number of cytoplasmic vacuoles and vesicles located outside the nucleus in a region corresponding to the Golgi apparatus. In particular, the vesicular transport of the clay inside the cells is more evident in hTERT RPE-1 cells, this transport is useful for conveying materials to the various compartments of the cell. Furthermore, after 24 h of incubation, the adsorption of the nanomaterial did not damage neither the cells nor the cell membranes.

*2.2. Study of the internalization pathway of Ht/**1Cl** by fluorescence microscopy*

By MTS cytotoxicity assays we have previously verified that treatment with inhibitors of different cellular transport pathways did not inhibit cell viability (data not shown). We evaluated both the mechanisms of Ht uptake into the cells and the transport called intracellular vesicular transport that

conveys materials to the various compartments of the cells. It is known[21] that both processes involve energy expenditure for the cells, therefore, they are considered active transports. In particular to evaluate the processes involved in Ht cellular uptake and transport, different studies with several inhibitor pathways will be performed. In this regard, we evaluated the effect of the following inhibitors: *i*) sodium azide which is commonly used to deplete cellular ATP levels and to generally inhibit endocytosis or all energy-dependent processes; *ii*) Chlorpromazine H typically used as inhibitors of clathrin-mediated endocytosis; *iii*) Nocodazole that is a pharmacological inhibitor of microtubule polymerization, which is responsible for a variety of cell movements, including intracellular transport and for this reason is used to determine the role of microtubules; and *iv*) Cytochalasin D which induces the depolymerization of f-actin. Figure 3 shows the images obtained under treatment of the cells with the several inhibitors investigated. As it is possible to observe the cellular absorption of Ht is not reduced by any treatment but depending on the treatment a different intracellular distribution occurs. Certainly ATP-dependent intracellular transport mechanisms are involved, as can be seen from the diffuse distribution of Ht, compared to the control, after treatment with sodium azide. As already reported for other clays, both microtubules and actin filaments participate in the cellular trafficking of Ht as well (Figure 3D-E).[17]

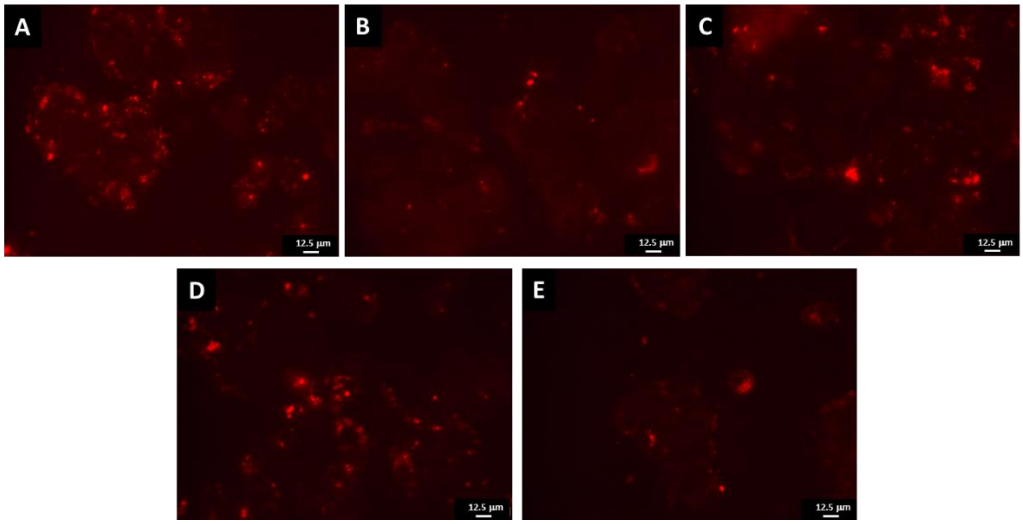

Figure 3. Fluorescence microscopy images of inhibition of Ht/**1Cl** internalization in MCF-7 cells. The cells were treated with: A) no inhibitors; B) Sodium azide 0.005%; C) Chlorpromazine H 10 µg/mL, D) Nocodazole 10 µM; E) Cytochalasin D 10 µM) for 2 h 30′ and then incubated with Ht/**1Cl** nanomaterial for 24 h. Scale bar: 12.5 µm, objective 40×.

Covalent modification of Ht edges with methotrexate

Recently, some of us developed a novel prodrug system based on the combination of halloysite nanotubes and methotrexate (MTX), chosen as drug model. The obtained nanomaterial showed promising activity as cytotoxic agent towards leukemia cell lines.[22] Based on these results, herein we envisage the possibility to covalent graft MTX at Ht edges. The covalent approach was chosen

both because of no complexation occurs between MTX and Ht and for the higher degree of organosilane functionalization achieved at Ht edges in comparison to halloysite. The latter could be advantageous for future biological applications.

The covalent grafting between MTX and Ht was accomplished by a two-step procedure as reported in Scheme 1. First, the silanol groups present at the edges of Ht were reacted with an excess of 3-amino propyltrimethoxysilane (3-APMTS) to obtain Ht-NH_2 nanomaterial following a procedure reported elsewhere.[23] More specifically, the grafting of the organosilane at Ht edges was performed by microwave (MW) irradiation at 100 °C, in solvent free conditions, for an irradiation time of 1 h. After work-up, the degree of functionalization of Ht, estimated by TGA, was 1.03 mmol g^{-1}.

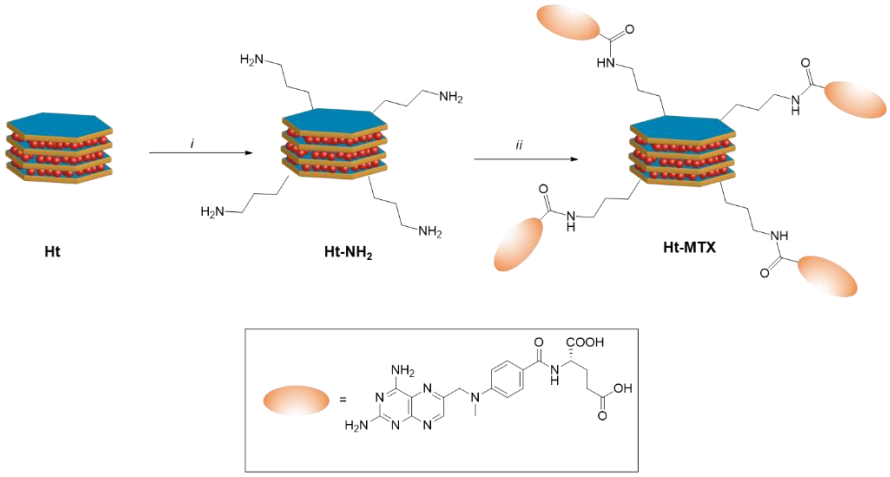

Scheme 1. Schematic representation of the synthesis of Ht-MTX nanomaterial. Synthetic route: (*i*) 3-APTMS, MW, solvent-free, 100 °C, 1 h; (*ii*) MTX, EDC·HCl, DMF, 48 h, r.t..

Afterwards, the Ht-MTX nanomaterial was obtained by the covalent grafting of MTX on Ht-NH_2 nanomaterial in DMF, using EDC as coupling agent, at room temperature for 4 days. After work-up the amount of MTX linked onto Ht, as estimated by TGA, was ca. 3.6 wt% with a degree of functionalization of 0.075 mmol g^{-1}. As it is possible to note, after MTX linkage, some unreacted amino groups are still present at Ht edges which could be useful to improve cellular uptake.

The Ht-MTX carrier system was thoroughly characterized by TGA, FT-IR spectroscopy, DLS and ζ–potential measurements. Furthermore, the morphology of the nanomaterial was imaged by Scanning Electron Microscopy (SEM) and HAADF/STEM investigations.

The TGA of Ht, reported in Figure 4a, shows a gradual and continuous decomposition process in the range 200-700 °C corresponding to the loss of physisorbed and hydration water present in the lamellar structure of the material up to reaching a constant weight equal to 91.63 wt%. Ht-NH_2 and Ht-MTX compounds undergo in the range ~300-700 °C degradation of the organic functionalities, with higher weight loss for Ht-MTX that reached constant weight of 79.12 wt%. On the basis of the thermogravimetric curves, the degree of functionalization of parent Ht after reaction with 3-APMTS and subsequent grafting of MTX on Ht-NH_2, was calculated as above reported.

FT-IR spectrum of Ht-MTX nanomaterial showed typical Ht vibration stretching bands and some stretching bands related to the drug. In particular, the bands at ca. 2980 and 2850 cm^{-1} related to stretching of methylene groups, the band at ca. 1650 cm^{-1}, which is superimposed to the typical band of Ht, due to the stretching of the amide C=O and the bands around 1483 and 1435 cm^{-1} due to the stretching of the C–N groups. Furthermore, it is also possible to observe a band at ca. 3320 cm^{-1} related to stretching of the N–H group of the amide bond.

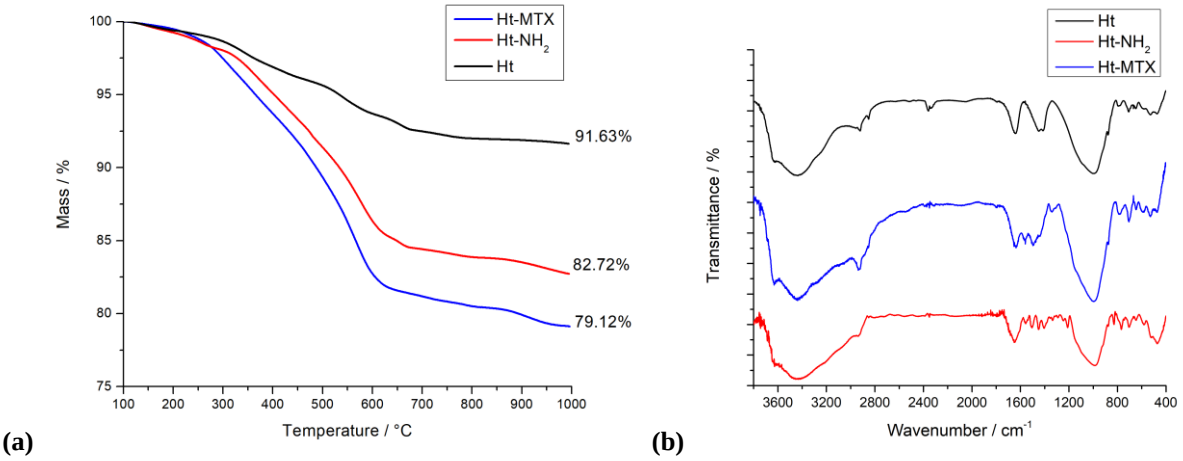

Figure 4. (a) Thermoanalytical curves and b) FT-IR spectra Ht, Ht-NH_2 and Ht-MTX nanomaterials.

The aqueous mobility of the nanomaterial was investigated by dynamic light scattering measurements (DLS). DLS experiments evidenced a hydrodynamic diameter of Ht-MTX is 520 ± 45 nm, value slightly higher than that of pristine Ht (432 ± 45 nm) in agreement with the introduction of an organic moiety at the Ht edges. As concerns the surface charge, the Ht-MTX nanomaterial presents a negative ζ-potential (-27 ± 3 mV). It should be noted that the net charge of the clay was slightly increased by the functionalization with MTX, being that the ζ-potential of pristine hectorite is -37 mV.[9]

SEM micrography (Figure 5A) clearly showed the covalent modification of hectorite did not affect its morphology. Similar conclusions can be drawn from HAADF-STEM investigations. As shown in Figure 5B, the Ht-MTX exhibits the typical morphology of hectorite (Figure 5b).[23] The EDS spectrum was also obtained by integration over the entire region and confirmed the presence of C and N atoms from the MTX grafted at the Ht edges besides the Mg, Si and O atoms related to the inorganic support (Figure 5C). Furthermore, EDS elemental mapping showed that the MTX molecules are mainly present at the edges of the nanodisks, as highlighted by the distribution of N atoms (Figure 5D).

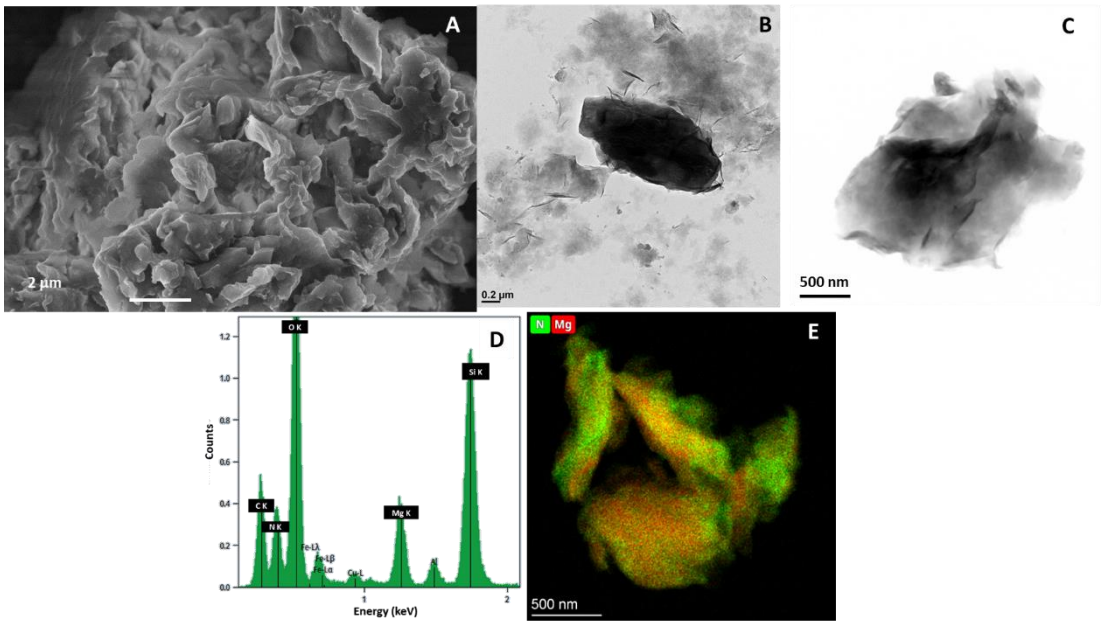

Figure 5. (a) SEM and (b-c) TEM images of (b) pristine Ht;[23] (c) Ht-MTX nanomaterial; (d) EDX spectrum; (e) EDX elemental mapping image.

To evaluate the performances of the Ht-MTX as carrier for antitumoral drugs, the kinetic release of MTX from it was evaluated by the dialysis bag method using conditions designed to mimic physiological conditions (HCl 1×10^{-3} M, pH 3.0; phosphate buffer 50 mM, pH 7.4) and the obtained kinetic data are shown in Figure 6. As it possible to note, a slow release of MTX was observed at pH 7.4 reaching ca. 50 wt% of the total MTX released after 24 h. Conversely, at pH 3.0 the MTX release was slow and sustained over the time. Lower amount of MTX is released at pH 3.0 than at pH 7.4 because of the different solubility of the drug in the two media. As already reported, MTX, being a dicarboxylic acid, is highly ionized, with two negative charges, at pH 7.4 (pK_{a1} = 4.8 and pK_{a2} = 5.5), which means that it leading to greater and faster dissolution and, subsequently, to a greater and faster release compared to pH 3.0. Therefore, after the amide bond hydrolysis the MTX released molecules at pH 7.4 can spread through the dialysis membrane, conversely their diffusion is limited at pH 3.0.

On the contrary, as reported elsewhere,[22] in the same pH conditions the free MTX spread through the dialysis membrane almost totally within 10 min and 1 h, at pH 7.4 and 3.0, respectively, according to the different drug solubility in the two media. This finding highlights the importance of the covalent linkage of MTX onto Ht edges to achieve a sustained and controlled release of the drug within the time.

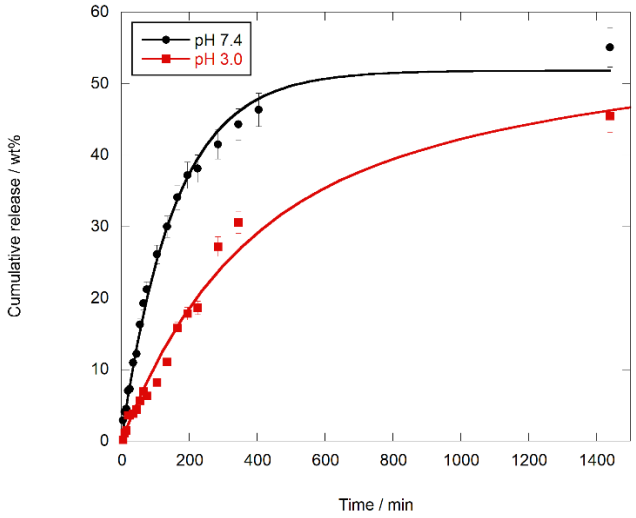

Figure 6. Kinetic release of MTX from Ht-MTX in HCl 1×10^{-3} M, pH 3.0 and phosphate buffer (0.05 M) solution at pH 7.4, at 37 °C. Reported are the mean ± SD values of three independent experiments.

To better understand the release mode, the experimental data were fitted by Power Fit, first-order and DEM models. The results showed that the kinetic data were better fitted, at pH 7.4, by first order model (M = 52 ± 1 wt%, k = 0.0064 ± 0.0003 min^{-1}, R^2 = 0.9933) in agreement with a diffusion of the drug through the dialysis membrane after the amide bond hydrolysis. Conversely, at pH 3.0 the kinetic data are better described by the double exponential model (R^2 = 0.9886). According to the literature, the DEM describes a mechanism consisting of two parallel reactions involving two distinguishable species. Based on these findings, we hypothesized that the slow hydrolysis of amide bond occurs (k_1 = 0.003 ± 0.0003 min^{-1}), but some MTX molecules released, due to their low solubility in the release medium, remain on the hydrophobic surface of Ht and slowly released within the time (k_2 = 0.0004 ± 0.0009 min^{-1}).

Cytotoxic studies

Finally, to exploit the possibility to use the synthetized Ht-MTX as potential anticancer system, the cytotoxic effects of the Ht-MTX were also evaluated on different cancer cell lines, namely acute myeloid leukemia (HL60) and its multidrug resistance variant (HL60-R), breast (MCF-7) and bladder (5637, UMUC3 and RT112) cancer cell lines. These cell lines were chosen since they present different characteristics, and therefore allowed us to expand the potential application fields of the Ht-MTX in the drug carrier field. The obtained resulted are reported in Figure S.1 and S.2, where data obtained with free MTX are also reported for comparison. Pristine Ht did not show any cytotoxicity in all range of concentration investigated. As it is possible to observe from Figure S.1 and S.2, the Ht-MTX nanomaterial exhibited a dose-dependent cytotoxic activity in all cell lines investigated with results comparable with free MTX. The MCF-7 cell line resulted the less sensitive to the treatment in comparison to the leukemia and bladder ones. The latter is in agreement with the

low efficacy of MTX in the treatment of breast cancer.[24] The obtained IC_{50} are reported in Table 1 and they show that the Ht-MTX nanomaterial is a promising agent for the tumor treatment.

Table 1. IC_{50} values of the Ht-MTX nanomaterial on the different cell lines.

Compound	**IC_{50}** (μM)
MCF-7	
MTX	11 ± 0.7
Ht-MTX	16 ± 4.2
HL-60	
MTX	0.0046 ± 0.0003[22]
Ht-MTX	0.006 ± 0.001
HL-60R	
MTX	26.5 ± 12.1[22]
Ht-MTX	22.0 ± 4.2
5637	
MTX	0.041 ± 0.024
Ht-MTX	0.055 ± 0.004
UMUC3	
MTX	0.073 ± 0.021
Ht-MTX	0.138 ± 0.08
RT112	
MTX	0.078 ± 0.019
Ht-MTX	0.069 ± 0.016

Conclusions

In-depth understanding of biological properties of Ht, including its cellular uptake and intracellular transport pathways is crucial for the future use of the clay.

Here, we have reported a systematic study about the cellular uptake of Ht both by confocal laser scanning microscopy (on normal hTERT RPE-1 cell lines and cancer MCF-7 ones) and by wide-field fluorescence microscopy. To achieve this goal, Ht was labelled with a fluorescent probe, **1Cl**, which possesses the peculiarity to emit in different regions of electromagnetic spectrum after appropriate external stimuli. CLSM images confirmed that the clay can penetrate cellular membrane localizing mainly in the perinuclear region. After 24 h of incubation, both cells showed a cellular reorganization due to the Ht accumulation in certain portion of the cells. By various endocytosis-inhibiting studies, coupled with wide-field fluorescence microscopy, it was possible to conclude

that, similarly to other clays, the mechanisms involved in the Ht internalization are ATP-dependent and related to microtubules and actin filaments. Furthermore, to prove the effectiveness of Ht for future application in the biological field we covalently modified the Ht edges with methotrexate molecules (MTX), chosen as model, to develop a Ht-MTX nanomaterial for potential cancer treatment. The Ht-MTX nanomaterials was characterized by thermogravimetric analysis, FT-IR spectroscopy, DLS and ζ-potential measurements which demonstrated the covalent linkage between the drug molecules and the clay. SEM and HAADF/STEM investigations showed that the typical morphology of Ht is preserved after the modification. In addition, the images showed MTX is mainly localized at the edges of Ht nanodisks, as highlighted by the distribution of N atoms extracted by the elemental analysis obtained by EDS measurements. The kinetic release in physiological conditions (phosphate buffer pH 7.4 and HCl 10^{-3} M, pH 3.0) showed that in both pH investigated a *plateau* was reached after 24 h. Finally, cytotoxic studies on different cancer cell lines showed that Ht-MTX possesses relevant antiproliferative activity and make it as promising nanomaterial for cancer treatment.

EXPERIMENTAL DETAILS

All reagents needed were purchased from Merck and used without further purification. Hectorite was kindly gifted by Tolsa Group Inc. (Madrid, Spain). Ht-NH_2 was synthesized as reported elsewhere. **1Cl** was synthesized following a literature procedure.[25]

FTIR spectra (KBr) were recorded with an Agilent Technologies Cary 630 FTIR spectrometer (Agilent Technologies, Santa Clara, CA, USA). Specimens for these measurements were prepared by mixing 5 mg of the sample powder with 100 mg of KBr.

Transmission electron microscopy (TEM) was performed by means of a FEI Titan G2 60–300 ultra-high-resolution transmission electron microscope (FEI, Lausanne, Switzerland) coupled with analytical electron microscopy (AEM) performed with a SUPER-X silicon-drift windowless energy-dispersive X-ray spectroscopy (XEDS) detector. AEM spectra were saved in mode STEM (scanning transmission electron microscopy) with a HAADF (high angle annular dark field) detector. X-ray chemical element maps were also collected.

The thermogravimetric analysis (TGA) of the material was performed in a TGA/DSC1 STAR System from Mettler Toledo Inc. The sample (15 mg) was subjected to a pre-treatment in air flow (30 mL/min) from 25 °C to 100 °C with a heating rate of 10 °C/ min and holding time at 100 °C for 30 min, in order to remove any eventual physisorbed water. Then, the temperature was increased from 100 to 1000 °C under air flow (30 mL/min) and the weight loss occurring during this step was considered for calculating the organic weight content of the HNTs based nanomaterial.

The size analysis, ζ-potential and polydispersity index of the samples were determined using a Malvern Zetasizer Nano ZS instrument, fitted with a 532-nm laser at a fixed scattering angle of 173°C.

Scanning electron microscopy (SEM) images were acquired with a GEMINI (FESEM) CARL Zeiss coupled to an EDX microanalyser (Oxford Instruments). Samples were dried at 40 °C for a minimum of 48 h. Then, powdery samples were mounted over standard aluminum stubs and coated with carbon. Textural microphotographs were obtained at 3 kV, while EDX were acquired at 15 kV. In both cases, immersion lens detector was used (InLens, Zeiss).

Synthesis of Ht-MTX

MTX (50 mg, 0.12 mmol) was suspended in DMF (10 mL), and 1- Ethyl-3-(3′ -dimethylaminopropyl)carbodiimide (EDC HCl) (35 mg, 0.15 mmol) was added. The suspension was stirred under an argon atmosphere at room temperature for 10 min. Then, Ht-NH_2 (100 mg) was quickly added. The mixture was stirred for 48 h. Then, the solvent was removed by filtration; the powder was then rinsed successively with H_2O and CH_2Cl_2 and finally dried at 80 ◦C under vacuum.

Kinetic Release

The release of MTX from Ht-MTX was done as follows: ca. 20 mg of the sample were dispersed in 1 mL of dissolution medium (phosphate buffers (0.05 M) and HCl 1×10^{-3} M at pH 3.0 and 7.4, respectively) and transferred into a sealed dialysis membrane (Medicell International Ltd MWCO 12–14000 with a diameter of 21.5 mm). Subsequently the membrane was put in a round bottom flask containing 9 mL of the release medium at 37 °C and stirred. At fixed time, 1 mL of the release medium has been withdrawn and analysed by UV–vis measurements. To ensure sink conditions, 1 mL of fresh solution has been used to replace the collected one. Total amounts of drug released (F_t) were calculated as follows:

$$F_t = V_m C_t + \sum_{t=0}^{t-1} V_a C_i \qquad \text{(Eq. 1)}$$

where V_m and C_t are the volume and the concentration of the drug at time *t*. V_a is the volume of the sample withdrawn and C_i is the drug concentration at time *i* ($i < t$).

Cell Lines and Cell Growth Assays (MCF-7, HL-60, HL-60R)

The cell lines HL-60 and MCF-7 were obtained from ATCC®(CCL-240 and HTB-22, respectively, Rockville, MD, USA), while the variant HL-60R were cultured as previously described.[26] HL-60

and HL-60R cells were cultured in Roswell Park Memorial Institute (RPMI) 1640, while MCF-7 cells in Dulbecco's Modified Eagle's Medium (DMEM), both supplemented with 10% heat-inactivated fetal calf serum, 2 mM L-glutamine, 100 units/mL penicillin and 100 μg/mL streptomycin (all reagents were from HyClone Europe Ltd., Cramlington, UK) in a humidified atmosphere at 37 ˚C in 5% CO_2. Human bladder cancer cell lines RT112, 5637 and UMUC3 were maintained in RPMI 1640 supplemented with 10% fetal calf serum (FCS), 2 mM L-glutamine ,100 U/mL penicillin and 100 μg/mL streptomycine-sulphate.

The cells were seeded at 5×10^3 cells/well onto 96-well plates and incubated overnight at 37 °C. At time 0, the medium was replaced with fresh complete medium supplemented with the synthetized nanomaterials. Following 72 h of treatment, 15 μL commercial solution obtained from Promega Corp. (Madison, WI, USA) containing 3-(4,5-dimethylthiazol-2-yl)-5-(3-carboxymethoxyphenyl)-2-(4-sulphophenyl)-2H-tetrazolium (MTS) and phenazine ethosulfate was added. The plates were incubated in a humidified atmosphere at 37 ˚C in 5% CO_2 for 2 h, and the bioreduction of MTS dye was evaluated by measuring the absorbance of each well at 490 nm using a microplate absorbance reader (iMark Microplate Reader; Bio-Rad Laboratories, Inc., Hercules, CA, USA). Cell growth inhibition was expressed as a percentage of the absorbance of the control cells. In the case of bladder cancer cell lines cell viability was quantified by 3-(4,5-dimethylthiazol-2-yl)-2,5-diphenyltetrazolium bromide staining (MTT) (working solution 0.5 μg/mL). After 1 h of incubation, the supernatants were removed, the formazan crystals were dissolved with dimethyl sulfoxide and the absorbance at 570 nm was measured using a microtiter plate reader.

The cytotoxicity was evaluated as IC_{50}, shown as a mean ± SD from three independent experiments.

Confocal Laser Scanning Microscopy

Confocal images were acquired with an OlympusFluoView10i confocal laser scanning microscope (Olympus, Japan) using a 60 × objective at 37 °C. The hTERT RPE-1-immortalized retinal pigment epithelial cell line and MCF-7 breast cancer cell line used in this study were cultured in DMEM medium supplemented with 1% glutamine, 10% heat- inactivated fetal bovine serum and 100 U/mL penicillin and 100 lg/mL streptomycin. Cells were seeded on chamber slide system at a density of 10.000 cells/well containing 300 μL of complete medium and incubated overnight at 37 °C in a humidified 5% CO_2 atmosphere. After 24 h, the medium was replaced with a fresh complete medium and the cells were treated with an aliquot of Ht/1Cl dispersed in water. Measurement was acquired using laser excitation at 405 nm or 595 nm. Emitted fluorescence was acquired in photon-counting mode.

Internalization pathway of Ht/**1Cl** was studied by fluorescence microscopy. MCF-7 cells were seeded at a density of 2×10^4 cells per well on chamber slide for cell culturing and incubated for 24 h at 37 °C in 5% CO_2. Subsequently, cells were treated for 2 h 30′ with Chlorpromazine

Hydrochloride (10 μg/mL), Cytochalasin D (10 μM), Nocodazole (10 μM) and Sodium azide 0.005%. After finished the treatment, cells were washed with phosphate buffer saline 1X (PBS-1X) and then Ht/1Cl was added for 24 h. At the end, cells were washed with PBS-1X and fixed with 4% paraformaldehyde for 20 minutes. After this passage cells were washed with PBS-1X and nuclei were stained with 1 μg/mL of the nuclear stain DAPI (4′,6-diamidino-2-phenylindole) (Invitrogen) for 20 minutes. After nuclear staining, cells were further washed with PBS 1X, and the slide was observed under fluorescence microscope.

Acknowledgements

The work was financially supported by the University of Palermo. This work was carried out in the frame of the PON ‘‘AIM: Attrazione e Mobilità Internazionale” No. 1808223-1 project. Confocal measurements were performed at ATeN Center – University of Palermo.

References

1. M. Massaro, C. G. Colletti, G. Lazzara and S. Riela, *J. Funct. Biomater.*, 2018, **9**.
2. M. I. Carretero and M. Pozo, *Appl. Clay Sci.*, 2009, **46**, 73-80.
3. A. Macgregor, *Geological Society, London, Special Publications*, 2013, **375**, 113-136.
4. M. C. da Rocha, T. Galdino, P. Trigueiro, L. M. C. Honorio, R. de Melo Barbosa, S. M. Carrasco, E. C. Silva-Filho, J. A. Osajima and C. Viseras, *Pharmaceutics*, 2022, **14**, 796.
5. A. Vikulina, D. Voronin, R. Fakhrullin, V. Vinokurov and D. Volodkin, *New J. Chem.*, 2020, **44**, 5638-5655.
6. A. Stavitskaya, E. Khusnetdenova, V. Vinokurov, Y. Lvov and R. Fakhrullin, *Chem. Commun.*, 2022, **58**, 7719-7729.
7. A. Stavitskaya, M. Rubtsova, A. Glotov, V. Vinokurov, A. Vutolkina, R. Fakhrullin and Y. Lvov, *Nanoscale Advances*, 2022, **4**, 2823-2835.
8. J. Zhang, C. H. Zhou, S. Petit and H. Zhang, *Appl. Clay Sci.*, 2019, **177**, 114-138.
9. G. Biddeci, G. Spinelli, M. Massaro, S. Riela, P. Bonaccorsi, A. Barattucci and F. Di Blasi, *Int. J. Nanomed.*, 2021, **16**, 4755-4768.
10. C. G. Colletti, M. Massaro, G. Lazzara, G. Cavallaro, S. Milioto, I. Pibiri, R. Noto and S. Riela, *Applied Clay Science*, 2020, **187**.
11. L. Delavernhe, M. Pilavtepe and K. Emmerich, *Appl. Clay Sci.*, 2018, **151**, 175-180.
12. N. Hegyesi, R. T. Vad and B. Pukánszky, *Appl. Clay Sci.*, 2017, **146**, 50-55.
13. A. Hoppe, N. S. Güldal and A. R. Boccaccini, *Biomaterials*, 2011, **32**, 2757-2774.
14. Z. Long, Y.-P. Wu, H.-Y. Gao, Y.-F. Li, R.-R. He and M. Liu, *Bioconjugate Chem.*, 2018, **29**, 2606-2618.
15. Y. Long, Y. Feng, Y. He, B. Luo and M. Liu, *ACS Appl. Nano Mater.*, 2022, **5**, 5813-5825.
16. X. Zhao, C. Zhou and M. Liu, *Journal of Materials Chemistry B*, 2020, **8**, 838-851.
17. H. Liu, Z.-G. Wang, S.-L. Liu, X. Yao, Y. Chen, S. Shen, Y. Wu and W. Tian, *J. Mater. Sci.*, 2019, **54**, 693-704.
18. M. Massaro, E. Licandro, S. Cauteruccio, G. Lazzara, L. F. Liotta, M. Notarbartolo, F. M. Raymo, R. Sánchez-Espejo, C. Viseras-Iborra and S. Riela, *J. Colloid Interface Sci.*, 2022, **620**, 221-233.
19. M. Massaro, M. Notarbartolo, F. M. Raymo, G. Cavallaro, G. Lazzara, M. M. A. Mazza, C. Viseras-Iborra and S. Riela, *ACS Appl. Nano Mater.*, 2022, DOI: 10.1021/acsanm.2c00603.
20. Z. Long, Y.-P. Wu, H.-Y. Gao, J. Zhang, X. Ou, R.-R. He and M. Liu, *Journal of Materials Chemistry B*, 2018, **6**, 7204-7216.
21. J. S. Bonifacino and B. S. Glick, *Cell*, 2004, **116**, 153-166.

22. M. Massaro, P. Poma, G. Cavallaro, F. García-Villén, G. Lazzara, M. Notarbartolo, N. Muratore, R. Sánchez-Espejo, C. Viseras Iborra and S. Riela, *Colloid Surf. B.*, 2022, **213**.
23. M. Massaro, C. Viseras Iborra, G. Cavallaro, C. G. Colletti, F. García-Villén, G. Lazzara and S. Riela, *Nanomaterials*, 2021, **11**, 506.
24. C.-W. Wu, H.-C. Liu, Y.-L. Yu, Y.-T. Hung, C.-W. Wei and G.-T. Yiang, *Oncol. Rep.*, 2017, **37**, 2177-2184.
25. E. Deniz, S. Sortino and F. M. Raymo, *The Journal of Physical Chemistry Letters*, 2010, **1**, 3506-3509.
26. P. Poma, M. Labbozzetta, P. Zito, R. Alduina, A. V. Ramarosandratana, M. Bruno, S. Rosselli, M. Sajeva and M. Notarbartolo, *Molecules*, 2019, **24**, 2871.